www.elsevier.com/locate/talanta

An electrochemiluminescence biosensor for detection of CdkN2A/p16 anti-oncogene based on functional electrospun nanofibers and core-shell luminescent composite nanoparticles

Xiaoying Wang, Yijie Wang, Yanqun Shan, Meng Jiang, Miao Gong, Xin Jin, Xiaoning Wang, Jie Cheng

PII: S0039-9140(18)30499-5
DOI: https://doi.org/10.1016/j.talanta.2018.05.033
Reference: TAL18673

To appear in: *Talanta*

Received date: 13 July 2017
Revised date: 28 April 2018
Accepted date: 8 May 2018

Cite this article as: Xiaoying Wang, Yijie Wang, Yanqun Shan, Meng Jiang, Miao Gong, Xin Jin, Xiaoning Wang and Jie Cheng, An electrochemiluminescence biosensor for detection of CdkN2A/p16 anti-oncogene based on functional electrospun nanofibers and core-shell luminescent composite nanoparticles, *Talanta,* https://doi.org/10.1016/j.talanta.2018.05.033

An electrochemiluminescence biosensor for detection of CdkN2A/p16 anti-oncogene based on functional electrospun nanofibers and core-shell luminescent composite nanoparticles

Xiaoying Wang[1], Yijie Wang[1], Yanqun Shan[1], Meng Jiang[1], Miao Gong[1], Xin Jin[1], Xiaoning Wang[2], Jie Cheng[3]

[1]*Key Laboratory of Environmental Medicine and Engineering, Ministry of Education, School of Public Health, Southeast University, Nanjing 210009, China*

[2]*Department of Hematology, the First Affiliated Hospital of Xi'an Jiaotong University, Xi'an 710061, China*

[3]*Department of oral and maxillofacial surgery, Affiliated hospital of stomatology, Nanjing M edical University, Nanjing 710061, China*

[*]Corresponding authors: Tel.: +86 25 83272563; fax: +86 25 83324322, wxy@seu.edu.cn

Abstract An electrochemiluminescence (ECL) biosensor based on functional electrospun nanofibers for hybridization detection of specific CdkN2A/p16 anti-oncogene at trace level *via* binding luminescent composite nanoparticles for signal amplification has been developed. The carboxylated multiwalled carbon nanotubes (MWCNTs) doped polycaprolactam 6 (PA6) electrospun nanofibers (PA6-MWCNTs) was prepared *via* electrospinning, which served as the nanosized backbones for silica nanoparticles (SiO_2) electrodeposition. The functional electrospun nanofibers (PA6-MWCNTs-SiO_2) used as supporting scaffolds for single-stranded DNA1 (ssDNA1) immobilization can dramatically increase the amount of DNA attachment and the sensitivity of hybridization. The sandwich construction of ssDNA1-CdkN2A/p16 anti-oncogene -tri(2,2'-bipyridyl)ruthenium(II) ($Ru(bpy)_3^{2+}$)/silver nanoparticles (AgNPs) doped gold (Au) core-shell luminescent composite nanoparticles (RuAg@AuNPs)-labeled ssDNA2 (RuAg@Au-ssDNA2) was fabricated through a hybridization reaction. It was observed that high amount of doped $Ru(bpy)_3^{2+}$ in RuAg@AuNPs successfully amplify the recognition signal by adding tripropylamine (TPrA). The change of ECL intensity was found to have a linear relationship in respect to the logarithm of the CdkN2A/p16 anti-oncogene concentrations in the wide range of 1.0×10^{-15}~1.0×10^{-12} M, with a detection limit of 0.5 fM (S/N=3) which is

comparable or better than that in reported anti-oncogene assays. Excellent sensitivity and selectivity make the developed biosensor a promising tool for the detection of tumor biomarkers.

Graphical Abstract:

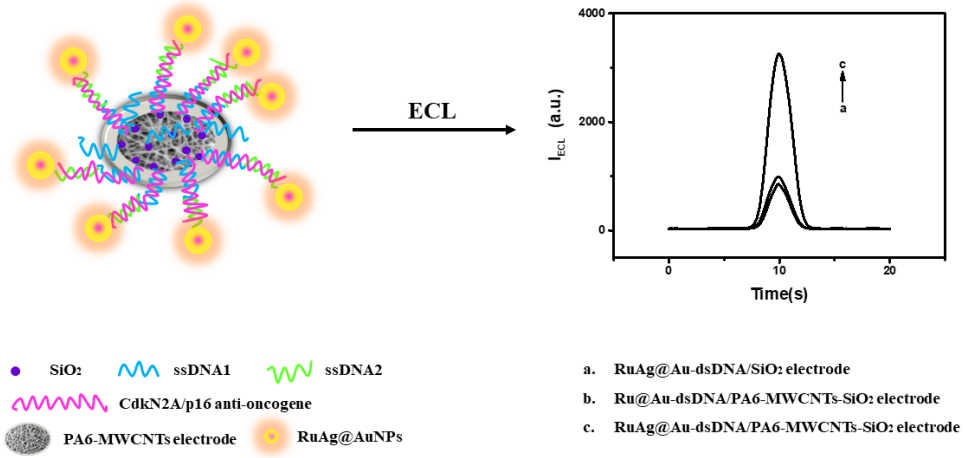

Keywords functional electrospun nanofibers, CdkN2A/p16 anti-oncogene, luminescent composite nanoparticles, a sandwich format, signal amplification

1. Introduction

The CdkN2A/p16 anti-oncogene, well known as multiple tumor suppressor 1 (MTS1) gene, is discovered by Kamb [1] in Cold Spring Harbor Laboratory in 1994. The Human genome organization (HUGO) officially named it cyclin-dependent kinase inhibitor 2A (CdkN2A). The overall length of CdkN2A/p16 anti-oncogene is 8.5 kb, which located and mapped on the short arm of chromosome 9, comprised of two introns and three exons (126bp, 307bp, 11bp, respectively [2]). The CdkN2A/p16 anti-oncogene, as a participant of cell cycle regulation, is

discovered by homozygous deletion, nonsense, missense or frame shift mutation in a large amount of carcinogenesis [3-5]. It is closely related to progression and malignancy of tumors. Therefore, special recognition and quantitative detection of CdkN2A/p16 anti-oncogene is extremely important in fundamental researches and clinical applications.

To date, a variety of conventional technologies have been developed to evaluate the status of CdkN2A/p16 anti-oncogene, such as direct DNA sequencing technology (DS) [6], denaturing gradient gel electrophoresis (DGGE) [7], polymerase chain reaction-restricted fragment length polymorphism (PCR-RFLP) [8], single-stranded conformation polymorphism (SSCP) [9], immunohistochemistry (IHC) [10], etc. They have offered useful and powerful tools in studying/screening the phenomenon of homozygous deletions and point mutations. However, the present methods are still faced with common drawbacks including semiquantitative at best, time-consuming, low sensitivity, complex operation, high cost and so on. Biosensing technologies having the advantages of high-sensitivity, simplicity, fast-response, low-cost and compatibility with micro fabrication technologies have been widely employed to achieve the accurate quantitative detection of related products of the CdkN2A/p16 anti-oncogene compared to the conventional methods [11-13]. At present, the point mutations of the CdkN2A/p16 anti-oncogene have not been reported at all, and the products reported in the literature are focus on methylation and protein of the CdkN2A/p16 anti-oncogene. In the first case, the biosensors can translate the methylation genetic recognition event into a corresponding analytical signal through optical [14,15] and electrochemical [16, 17] methodologies. In the second case, among the great varieties of transduction techniques, piezoelectric [13] and electrochemical [18] methodologies have evolved as versatile and powerful techniques for accurate immunosensing of p16 protein. Electrochemiluminescence (ECL), the generation of an optical signal triggered by an electrochemical reaction, has outstanding advantages, such as versatility, simplified optical setup, very low background signal, as well as good temporal and spatial control [19]. It has become an excellent and valuable detection technology in biosensors during the past several decades [20]. However, to our best knowledge, ECL biosensor has never been applied to detect the related products of the CdkN2A/p16 anti-oncogene.

As an important factor to develop a biosensor device, the amount and stability of the

biological recognition molecule was very vital. Although the field of ECL biosensors has grown considerably and a great number of different detection methods and strategies are available in the past decade [21-23], the researchers still think it is a big challenge that how to make the biological recognition molecule utmost and stability immobilizing on the supporting scaffolds [24, 25]. Nanofibers produced by electrospinning technology have received much attention on their unique physical and chemical properties [26]. Compared with the conventional planar materials, the nanofibers can flexibly regulate surface morphology with high porosity, uniform aspect ratio, mechanical strength and large surface areas [27]. Several reports have investigated the development of electrospun nanofiber-based biosensing platforms for biomolecular detection, such as glucose [28, 29], enzyme [30], nucleotide [31] and protein [32]. It is a good choice for highly sensitive biosensing applications to combine with electrospun nanofibers.

In recent years, our group have done a lot of researches on the preparation of electrospun nanofibers [33-37]. We functionalized electrospun nanofibers by electropolymerization of intrinsic conducting polymers, such as pyrrole, thionine and aniline. The functional composite electrospun nanofibers with the unique 3D nanostructure, large specific surface area and good biocompatibility used as supporting scaffolds for biological recognition molecule immobilization can dramatically increase the amount of molecule attachment and the detection sensitivity. So far, we have prepared a variety of electrochemical biosensors based on functional composite electrospun nanofibers to detect tumor biomarkers, such as p53 gene [35], k-ras gene [36] and p53 protein [37]. Herein, a novel approach of functionalization of electrospun nanofibers has been proposed. The multiwalled carbon nanotubes (MWCNTs) doped polycaprolactam 6 (PA6) electrospun nanofibers (PA6-MWCNTs) was prepared *via* electrospinning. Then the PA6-MWCNTs served as the nanosized backbones for nano-silica particles (SiO_2) electrodeposition. The functional electrospun nanofibers (PA6-MWCNTs-SiO_2) was obtained successfully for the first time.

The core-shell composite nanoparticles can be formed that a nanometer material covered with another nanometer material by chemical bonds or another affinity. Because of its unique property, the core-shell composite nanoparticles differ from the single substance, and are intensely studied in the past decades. The luminescence materials, such as tri(2,2'-bipyridyl)ruthenium(II) ($Ru(bpy)_3^{2+}$), luminol, etc. can be doped into the core-shell composite nanoparticles. Some

properties of the luminescence material can be changed through the formation of core-shell structure, such as luminous intensity and stability. It was not the simple component adduct behavior to change these properties, while it was a synergistic effect of the multi-components complex. Hence core-shell luminescent composite nanoparticles are ideal choices of biomolecule label for ECL biosensors, and a new approach to the new material design has been opened up. In this paper, $Ru(bpy)_3^{2+}$-silver nanoparticles (AgNPs) doped gold (Au) core-shell luminescent composite nanoparticles (RuAg@AuNPs) were prepared by low-temperature method.

Herein, on the basis of the original work [35, 36], we provided another successful example to demonstrate that the electrospun nanofibers could be used to develop highly efficient DNA-based ECL biosensor for sensitive determination of CdkN2A/p16 anti-oncogene. The functional electrospun nanofibers (PA6-MWCNTs-SiO_2) with the large specific surface area were served as the supporting scaffolds to carry the ssDNA1. The ECL biosensor was formed by coupling with the CdkN2A/p16 anti-oncogene and RuAg@AuNPs labeled ssDNA2, successively. In fact, the combination of functional electrospun nanofibers and core-shell luminescent composite nanoparticles can result in enormous signal amplification, and thereby, it makes the ECL biosensor achieve high sensitivity. An experimental schematic representation is illustrated in Fig. 1. In this paper, the characteristics of the sensing system for detection of the CdkN2A/p16 anti-oncogene and the analytical performance were examined.

2. Experimental section

2.1. Reagents and apparatus

The DNA oligonucleotides as shown in Table 1 in this study were obtained from Sangon Biotechnology (China). Polycaprolactam 6 (PA6) (weight average molecular weight ~20,000 g/mol, viscosity 2.2) was purchased from Debiochem (China). Carboxylated multiwalled carbon nanotubes (MWCNTs), the diameter of 40-60 nm and the length of 1-10 μm, were obtained from Shenzhen Nanotech Port Co. Ltd. (China). Tetraethylorthosilicate (TEOS) and trimethoxysilylpropy-diethylenetriamine (DETA) were purchased from United Chemical Technologies (Bristol, PA). $Ru(bpy)_3^{2+}$ (99.95%), tripropylamine (TPrA), $HAuCl_4{\cdot}3H_2O$ were

purchased from Sigma (USA). Others were all analytical reagents. All of the solutions were prepared with ultrapure water by a Millipore Milli-Q system.

The transmission electron microscope (TEM) images were recorded using JEM-2100F (JEOL, Japan). The fluorescence photographs were recorded using IX71-F22FL/PH inverted fluorescence microscope (Olympus, Japan). The Field Emission Scanning Electron Microscopy (FESEM) images were recorded using an S-4800 FESEM microscope (JEOL, Japan). ECL was measured with MPI-E electrochemiluminescence analyzer (Remax Electronic Science Tech. Co. Ltd., China), cyclic voltammetry (CV), electrochemical impedance spectroscopy (EIS) and differential pulse voltammetry (DPV) were recorded with a CHI 660D electrochemical analyzer (CHI instruments Inc., Chenhua Corp., China).

2.2. Preparation of PA6-MWCNTs-SiO_2 electrode

The preparation of the nanofibers electrode was similar to previously published protocols [38]. In brief, the surface of glassy carbon electrode (GCE) was handled by carefully polishing with alumina powder with particle size of 0.3 μm, rinsing with water and ethanol in an ultrasonic bath briefly and drying at room temperature, successively. PA6 (31 wt%) and MWCNTs (1 wt%) were dissolved in a mixture of cresol and formic acid (6:4, v/v) to obtain a homogeneous solution under the vigorous stirring for 12 h at room temperature. Electrospinning was carried out with a 20 mL syringe (1.2 mm diameter spinneret) at an electrical potential of 17 kV over a 20 cm gap between the spinneret and the clean GCE surface at a rate of 0.1 mL/h. The ambient temperature and relative humidity for electrospinning were kept at 25℃ and down to 40%, respectively. It took 3 min to deposit a nanofiber mat on the surface of the electrode that was marked as the PA6-MWCNTs electrode.

Two different nano-silica particles (SiO_2)-modified electrodes were prepared as follows: (1) The PA6-MWCNTs-SiO_2 electrode. SiO_2 were deposited onto the PA6-MWCNTs electrode by a multi-potential step electrodeposition technique in 1% fresh TEOS solution containing 5% MWCNTs with ultrapure water and ethanol (1:1, v/v) at room temperature. In brief, this procedure applied a reduction potential (-2 V) for a fixed period (40 s), followed by a relaxation potential (-0.4 V for 80 s) in 5 repeated cycles, initial potential 0 V, sampling interval 0.002 s and static time 2 s. A modest stir was going on through the electrodeposition. The electrode was washed with 10

mM PBS (pH 7.2) thoroughly. The as-prepared electrode was denoted as PA6-MWCNTs-SiO_2 electrode. (2) The SiO_2 electrode. The SiO_2 was modified on the bare GCE with the same processes as (1). The as-prepared electrode was denoted as the SiO_2 electrode.

2.3. Preparation of RuAg@AuNPs labelled ssDNA2 probes

Core-shell nanoparticles composed of a core of Ag and a thin layer of Au shell (Ag@Au) were synthesized with a low-temperature method through minor revision of the literature [39]. Silver nanoparticles (AgNPs) were prepared by $NaBH_4$ reduction of $AgClO_4$ in the presence of trisodium citrate ($Na_3C_6H_5O_7$). In brief, 1mL of 0.01 M $AgClO_4$ was rapidly added to 99 mL fresh mixed solution containing 1.0 mM $NaBH_4$ and 0.3 mM $Na_3C_6H_5O_7$ in the ice-bath, with the violent stirring at 30 min to room temperature, gradually forming a bright yellow colloid solution. Adding to a certain amount of sodium dodecyl sulfate (SDS) which was made the concentration up to 0.3 mM for steadying colloid and preventing aggregation. The colloid was then purified by centrifugation and redispersed in ultrapure water.

Two different core-shell luminescent composite nanoparticles were prepared as following: (1) RuAg@AuNPs. 1 mL AgNPs (The concentration of the AgNPs was calculated to be 0.7 mM using anodic stripping voltammetric technology at +0.35 V (vs. Ag/AgCl) with 1 μM $AgNO_3$ as a standard according to the literatures [40]), 40 mM $Ru(bpy)_3^{2+}$ were dispersed evenly in 100 mL of 0.3 mM $Na_3C_6H_5O_7$ solution. After that, gold shells, growing on the surface of the AgNPs, were simultaneously treated with 0.8 mg $HAuCl_4{\cdot}3H_2O$ and 3.7 mg $NaBH_4$ solution *via* dropwise addition at the ice-bath and violently stirred a while. After adding 30 μM SDS, the core-shell nanoparticles were purified by centrifugation and redispersed in ultrapure water. Then the products were stored in a dark glass bottle at 4℃ for further use. (2) Ru@AuNPs. The preparation processes of (2) and (1) are exactly the same, except that the AgNPs are not doped during the preparation. The Ru@AuNPs were stored in a dark glass bottle at 4℃ for further use.

3'-SH-capped 1 μM ssDNA2 was dissolved in 1 mL RuAg@AuNPs solution for 12 hours at 4℃, which was self-assembled on the surface of RuAg@AuNPs *via* Au-S bond. It was washed, centrifuged, resuspended in 10 mM PBS (pH 7.2). The RuAg@AuNPs labelled ssDNA2 probes (RuAg@Au-ssDNA2) were obtained. The concentration of the RuAg@Au-ssDNA2 was calculated to be 0.81 μM according to the value of ultraviolet (UV) absorption of the ssDNA2 at

260 nm. Then, RuAg@Au-ssDNA2 was stored at 4℃ for later use.

2.4. Fabrication of dsDNA electrode

Surface modification of PA6-MWCNTs-SiO_2 and covalent conjugation of oligonucleotides onto the SiO_2 nanoparticle surface were prepared according to the references [41,42]. In brief, the PA6-MWCNTs-SiO_2 electrode was immersed in 5.0 mL freshly prepared solution containing DETA (1%) and acetic acid (1.0 mM) for 30 min at room temperature. After rinsed with ultrapure water, the above amino-functionalized PA6-MWCNTs-SiO_2 electrode was reacted with 5.0 mL of glutaraldehyde (GA) solution (5%) for 2 h with shaking in a water bath of 37 ℃. After rinsed with ultrapure water, the above electrode was incubated with 1 μM of 5'-NH_2-capped ssDNA1 in 10 mM PBS (pH 7.2) for 2 h with stirring in a water bath of 37 ℃. Then the electrode was washed with 10 mM PBS (pH 7.2), and the ssDNA electrode was obtained.

Then the ssDNA electrode was immersed in 10 mM PBS (0.3 M NaCl, pH 7.2) containing a certain concentration of CdkN2A/p16 anti-oncogene and RuAg@Au-ssDNA2 with stirring 40 min in a water bath of 37 ℃. The as-prepared electrode was marked as dsDNA electrode.

2.5. ECL measurement

The ECL determinations were performed at room temperature in a 10 mL homemade quartz cell. A three-electrode system was used with the dsDNA electrode as the working electrode, an Ag/AgCl (sat.) as the reference electrode and a platinum wire as the counter electrode.

Cyclic voltammetry mode with continuous potential scanning from 0.0 to 1.2 V and scanning rate of 100 mV s^{-1} was applied to achieve ECL signal in 10 mM PBS containing 1.0 mM TPrA (pH 7.2). A high voltage of 800 V was supplied to the photomultiplier for luminescence intensity determination, unless explicitly stated, the magnification factor of the photomultiplier was set at 4. The ECL and CV curves were recorded simultaneously.

3. Results and discussion

3.1. The characterization of the core-shell luminescent composite nanoparticles

The micromorphologies of $Ru(bpy)_3^{2+}$/AgNPs doped Au core-shell luminescent composite nanoparticles (RuAg@AuNPs) prepared by a low-temperature method were analyzed by

transmission electron microscope (TEM) and inverted fluorescence microscope. As shown in Fig. 2A, the TEM images were composed of nanoparticles, which have well-defined shape and size, and slight aggregation. The RuAg@AuNPs were spherical in shape and extremely uniform in size of the average diameter being 70±10 nm. The results were further confirmed by fluorescence observations. The fluorescence photographs show that the RuAg@AuNPs emit bright orange light at 610 nm (as shown in the inset), which suggests that the RuAg@AuNPs maintain the optical property of $Ru(bpy)_3^{2+}$ ions in the core-shell structure of the composite.

The electrochemical characterizations of the RuAg@AuNPs were analyzed using DPV and ECL as shown in Fig. 2B. The DPV measurements were conducted for the RuAg@AuNPs (100 μL) and the $Ru(bpy)_3^{2+}$ solution (40 μM) in 10 mM PBS (pH 7.2) from 0.6 to 1.2 V with pulse amplitude 0.05 V, pulse width 0.05 s and pulse period 0.2 s. As shown in the Fig. 2B, two independent DPV peaks were clearly observed at potentials of approximately +0.78 V and +1.15 V versus Ag/AgCl (sat.) for the RuAg@AuNPs (curve a). The +0.78 V is the characteristic peak of Au according to the literature [43]. We found that the $Ru(bpy)_3^{2+}$ solution had an obvious peak at +1.15 V under the same conditions in the DPV curve (red dotted line circle, curve b). It is confirmed that the DPV behavior of $Ru(bpy)_3^{2+}$ had not changed, and $Ru(bpy)_3^{2+}$ was successfully loaded in a layer of Au shell. The ECL intensity-time curves of the RuAg@AuNPs were investigated and shown in the inset of the Fig. 2B. RuAg@AuNPs exhibited excellent ECL behaviors, including significant increase in intensity and stability. It might be attributed to the facts that the SDS (anionic surfaceactive agent) stabilized AgNPs carried a large amount of $Ru(bpy)_3^{2+}$ *via* electrostatic interaction and they were doped together in the Au shell, and $Ru(bpy)_3^{2+}$ molecules were insulated from quenching molecules (oxygen, phenolic compounds, etc.) [44] in the external environment. The ECL signal increases sharply at 0.9 V and reaches its peak at 1.15 V (Fig. 2C, ECL intensity-potential curves), which is almost the same as that of free $Ru(bpy)_3^{2+}$ under the same experimental conditions. These results are in agreement with the characteristics of free $Ru(bpy)_3^{2+}$ ion [45], which convinces that the RuAg@AuNPs properly maintain the electrical properties of the $Ru(bpy)_3^{2+}$ ions.

In order to demonstrate the advantage of the RuAg@AuNPs in ECL amplification, we compared the different ECL behaviors between Ru@AuNPs and RuAg@AuNPs (The preparation processes of them are exactly the same, except that the AgNPs are not doped during the

preparation of the Ru@AuNPs) in 10 mM PBS containing 1.0 mM TPrA (pH 7.2), respectively. As shown in Fig. 2C, the ECL behaviors of Ru@AuNPs and RuAg@AuNPs are similar, but the ECL signals of the RuAg@AuNPs (curve a) were about 3.4 times higher than that of the Ru@AuNPs (curve b). It might be attributed to the facts that RuAg@AuNPs contained a large number of $Ru(bpy)_3^{2+}$ with the assistance of AgNPs, and AgNPs could be a quasi-coreactant to enhance the ECL when $Ru(bpy)_3^{2+}$ was used as luminescent reagent [46]. A possible mechanism was proposed that AgNPs could react with $Ru(bpy)_3^{2+}$ to facilitate the formation of excited state of $Ru(bpy)_3^{2+*}$, $Ru(bpy)_3^{2+*}$ would relax radiation to the ground state and therefore the enhanced luminescence was observed. The ECL reactions of RuAg@AuNPs are described in Scheme 1 [46,47]. Thus, compared with Ru@AuNPs, the RuAg@AuNPs are more suitable as DNA labels in this experiment to amplify the ECL signal.

3.2. The characterization of the PA6-MWCNTs-SiO_2 electrode

In the paper, silica nanoparticles (SiO_2) were deposited onto the PA6-MWCNTs electrode *via* a multi-potential step electrodeposition technique. Such an electrochemically triggered pH change inducing the nanophase transition is now a well-established process [48,49]. In brief, the method involved the immersion of the PA6-MWCNTs electrode into a 1% fresh TEOS (precursor) solution containing 5% MWCNTs and the application of a cathodic potential likely to generate the basic catalysts (i.e., hydroxyl groups) at the electrode/solution interface, causing thereby a local pH increase resulting in the precursors' polycondensation (partially or completely) and concomitant growing of a nanophase materials silica. During the procedure, the normal hydrolysis and condensation of TEOS also took place slightly. Both steps are usually performed in "one pot".

The FESEM images and the diameter distribution diagrams of PA6-MWCNTs electrospun nanofibers and PA6-MWCNTs-SiO_2 electrode were showed in Fig. 3A and Fig. 3B, respectively. The PA6-MWCNTs electrospun nanofibers are uniform, smooth and without branch structures. The nanofibers aligned in random orientation and formed a porous 3D nanofibrous membrane structure (the inset of the Figure. 3A). The diameters of the nanofibers range from 50 nm to 300 nm (the inset of the Figure. 3B). The assembly of SiO_2 on PA6-MWCNTs electrospun nanofibers electrode can be observed in Figure. 3A. A large quantity of irregular-shaped SiO_2 were found to distribute uniformly and in high coverage density on the surface of the PA6-MWCNTs electrospun

nanofibers. Compared with the PA6-MWCNTs electrospun nanofibers, the diameter of the PA6-MWCNTs-SiO_2 increased from 200 nm to 500 nm as shown in Figure. 3B. In this case, PA6-MWCNTs electrospun nanofibers served as the nanosized backbones for SiO_2 electrodeposition, resulting in the SiO_2 covered around the PA6-MWCNTs electrospun nanofibers in a coarse structure. By this way, a significantly increasing of the SiO_2 amount around PA6-MWCNTs electrospun nanofibers was generated.

The electrochemical surface areas of various electrodes have been evaluated using Randles-Sevcik equation ($I_p = 2.69 \times 10^5$ A $D^{1/2}$ $n^{3/2}$ $v^{1/2}$ C, I_p: peak current, A: electrode area, D: diffusion coefficient (0.76×10^{-5} cm^2/s), n: electrons involved, v: sweep rate, C: concentration.) according to the reported protocols [50]. In brief, cyclic voltammetry mode with continuous potential scanning from -0.2 to 0.6 V and different scanning rate from 0.01 V/s to 0.1 V/s (the interval is 0.01 V / s) was applied to bare GCE, SiO_2 and PA6-MWCNTs-SiO_2 electrodes to achieve I_p signals in 5 mM $K_4[Fe(CN)_6]$ (probe molecule) in 0.1 M KCl, respectively. The slope of $I_p \sim v^{1/2}$ was the electrochemical surface area of the electrodes. The surface area was found to be 0.071, 0.171 and 0.684 cm^2 for the bare GCE, SiO_2 and PA6-MWCNTs-SiO_2 electrodes, as shown in Table 2. Compared with the bare GCE, the electrochemical surface area of the SiO_2 electrode significantly improved. It was consistent with the fact that SiO_2 with 3D structure produced by electrodeposition could effectively increase the specific surface area. The electrochemical surface area of the PA6-MWCNTs-SiO_2 electrode had a significant increase in contrast to the SiO_2 electrode. It was because that each PA6-MWCNTs electrospun nanofiber with a large surface area and conductivity which could be regarded as a quasi-independent modified electrode when the SiO_2 electrodeposition reaction on the surface of the PA6-MWCNTs electrode. Finally, the PA6-MWCNTs-SiO_2 electrode congregated the electrodeposition effects of a large number of modified electrodes and a huge electrochemical surface area was obtained.

Herein, the sensitivity of the CdkN2A/p16 anti-oncogene ECL biosensor was investigated using SiO_2 and PA6-MWCNTs-SiO_2 electrodes as supporting scaffolds for ssDNA1 immobilization, respectively. The fabricate process of the sandwich format of the ssDNA1-(CdkN2A/p16 anti-oncogene)-(RuAg@Au-ssDNA2) are exactly the same. As shown in the Fig. 3C, the ECL signal of the PA6-MWCNTs-SiO_2 electrode (curve c) were about 3.6 times stronger than that of the SiO_2 electrode (curve a). It might be attributed to the facts that

PA6-MWCNTs-SiO_2 electrode with larger electrochemical surface area can dramatically increase the amount of DNA attachment and the sensitivity of hybridization. The result show that the PA6-MWCNTs-SiO_2 electrode is better suited as the supporting scaffold for the ssDNA1 in this experiment than the SiO_2 electrode. Moreover, the detection situation of the PA6-MWCNTs-SiO_2 electrodes using Ru@AuNPs and RuAg@AuNPs as DNA labels was investigated, respectively. The ECL signals of the RuAg@AuNPs-dsDNA electrode (curve c) were remarkably stronger than that obtained of the Ru@AuNPs-dsDNA electrode (curve b) as shown in the Fig. 3C. Thus, a higher sensitivity of the CdkN2A/p16 anti-oncogene ECL biosensor was obtained by using PA6-MWCNTs-SiO_2 electrode as supporting scaffold and RuAg@AuNPs as DNA labels in this experiment.

3.3. CV and EIS behaviors of different modified electrodes

The fabrication processes of the electrochemiluminescence biosensor were characterized by CV and EIS using $[Fe(CN)_6]^{3-/4-}$. The corresponding CV curves of the electrodes were used for recording each immobilization step as shown in Fig. 4A. A pair of well-defined reduction/oxidation peaks was obtained by a bare GCE (curve a). Compared with the former, the voltammogram was observed at the PA6-MWCNTs electrode (curve c) which declined a slightly in the redox current. It is consistent with the fact that tiny MWCNTs produced the effect on the conductivity of the PA6, moreover MWCNTs could improve the mechanical stability and prolong the durability of nanofibers under operating conditions [51]. An increase was presented in the redox current for PA6-MWCNTs-SiO_2 electrode (curve b). The SiO_2 nanoparticles were densely formed around the PA6-MWCNTs electrospun nanofibers. It might be attributed to the fact that the facilitation in charge-transport characteristics of SiO_2 nanoparticles (which created because of conductivity effect and abundancy of MWCNTs attached/doped to SiO_2 nanoparticles) could greatly promote electron-transfer reactions of the electrode surface and led to the increase in the redox current. Once the ssDNA1 was adsorbed onto the PA6-MWCNTs-SiO_2 electrode by covalent binding, asymmetric and irreversible waves accompanied by a decline in the redox current were obtained for the ssDNA electrode (curve d). The ssDNA1 which had a single-strand nucleic acid with negative charges on its phosphate backbone, making an electrostatic repulsive force to $[Fe(CN)_6]^{3-/4-}$ to hinder the electron transfer, implying that ssDNA1 was successfully

immobilized onto the PA6-MWCNTs-SiO_2 electrode surface. After hybridization, the peak current was further decreased (curve e) because of the increasing in the number of nucleic acids.

EIS is a well-established technique in investigating the feature of the surface-modified electrodes. For EIS measurements, $[Fe(CN)_6]^{3-/4-}$ was utilized as the redox probe and Nyquist plots were used to evaluate the R_{et} for modified electrodes. As shown in Fig. 4B, a smaller R_{et} displayed on the bare GCE (curve a). When the PA6-MWCNTs electrospun nanofibers were deposited on the surface of the electrode, the R_{et} was increased (curve b). Owing to the conductivity of SiO_2 nanoparticles, the semicircle diameter of the PA6-MWCNTs-SiO_2 electrode was decreased (curve c). Once the ssDNA1 was adsorbed onto the PA6-MWCNTs-SiO_2 electrode, the R_{et} was significantly increased (curve d). After hybridization, the R_{et} was continued to increase (curve e). It was consistent with the fact that the layer of nucleic acid molecules can insulate and perturb the interfacial electron transfer between the electrode and the electroactive species ($[Fe(CN)_6]^{3-/4-}$) in solution. As a result, we can conclude that the proposed DNA biosensor was fabricated successfully. The change in the CV and EIS curves of the electrodes illustrated the successful modification of the PA6-MWCNTs-SiO_2 onto GCE. It also indicated that the interactions between the ssDNA (1 and 2) and the CdkN2A/p16 anti-oncogene arose successively.

3.4. The characterization of the electrochemiluminescence biosensors

The performance of the electrochemiluminescence biosensors was related to the stability of the ssDNA electrode. After 7 days of storage at 4 ℃, the ssDNA electrode was investigated by doing a consecutive cycles of cyclic potential measurement in $[Fe(CN)_6]^{3-/4-}$ solution. As shown in Fig. 5A, after 20 cycles, rather small changes (<2 %) in the current responses were observed for the given ssDNA electrode. The result indicated that the ssDNA electrode was a stable sensing platform. At the same time, it also suggested that the ssDNA sequence was firmly immobilized on the PA6-MWCNTs-SiO_2 electrode surface due to covalent linkage. The freshly prepared ssDNA electrode (Fig. 5B, group curves a) and the above ssDNA electrode (7 days of storage at 4 ℃, Fig. 5B, group curves b) used to hybridize with the target CdkN2A/p16 anti-oncogene, respectively. Then 97.1% of the initial ECL signal was remained. After 3 weeks, the response of ECL signal decreased gradually and maintained about 90.3 % of the initial value. According to the obtained results, 4 ℃ was suitable condition for storage of the ssDNA electrode and the stability of this

fabricated CdkN2A/p16 anti-oncogene biosensor is appropriate.

Herein, the binding specificity of the ECL biosensor to DNA sequence was investigated by the control hybridization experiments for complementary DNA (CdkN2A/p16 anti-oncogene), one-base mismatched DNA, three-base mismatched DNA, noncomplementary DNA and the blank. As shown in Fig. 6, the ECL intensity of the blank and noncomplementary sequence of the CdkN2A/p16 anti-oncogene were almost negligible (Fig. 6a and e). When the ssDNA electrode was hybridized with the three-base mismatched sequence of the CdkN2A/p16 anti-oncogene (Fig. 6d), the I_{ECL} was a bit raising. The one-base mismatched DNA (C/A mismatched) gives about 58 % signal compared to the complementary DNA (Fig. 6c). The largest ECL intensity was achieved by detecting CdkN2A/p16 anti-oncogene for the ssDNA electrode (Fig. 6b), indicating that the dsDNA had been successfully formed. The relative standard deviation (RSD) of the I_{ECL} of CdkN2A/p16 anti-oncogene (1 nM) by 6 times repeated measurements was 2.43%, displaying the good reproducibility of this method. The experiment was repeated three times to observe its reproducibility. It also explained that the ssDNA1, CdkN2A/p16 anti-oncogene and RuAg@AuNPs modified ssDNA2 maintained their activity and unique structure on the PA6-MWCNTs-SiO_2 electrode in the present protocol. In summary, the ECL biosensor demonstrated good performance, including higher stability, specificity and reproducibility.

3.5. Optimization of experimental conditions

In order to maximize the detection sensitivity of the proposed ECL biosensor, various conditions were optimized by single factor experiments. The depositing time of the PA6-MWCNTs electrospun nanofibers on the surface of the GCE was manipulated according to the previously published protocols [34]. The efficiency of the hybridization is in correlation with the ionic strength of the hybridization buffer, hybridization time and hybridization temperature. The ECL signal of RuAg@Au at +1.17 V versus Ag/AgCl (sat.) increased with the increase of the NaCl concentration and the hybridization time. It reached plateau regions at the NaCl concentration of 0.3 M and the hybridization time of 40 min. Thus, the optimal NaCl concentration and hybridization time were chosen at 0.3 M and 40 min. The curve that the ECL intensity varied with the hybridization temperature from 5 to 50 ℃ with an increment of 5 ℃ was like a parabola and its peak was about at 37 ℃. So, 37 ℃ was chosen as the optimal

hybridization temperature.

The detecting buffer solution has great impact on ECL signal of the RuAg@Au. In order to obtain the optimal ECL response, the effects of concentration of TPrA (ECL coreactant) and the pH of the buffer solution on ECL intensity were investigated. The ECL intensity varied with the concentration of the TPrA from 0 to 2.0 mM with an increment of 0.5 mM was like a parabola and its peak was at 1.0 mM. So, 1.0 mM was chosen as the concentration of the TPrA. The pH values of PBS solution in the range from 5.0 to 9.0 were considered in the study. The ECL intensity increased with the increase of pH values from 5.0 to 7.0 and then decreased in the range of 7.5 to 9.0, with a plateau in the range of 7.0 to 7.5. To generate an ECL signal at high efficiency, strong reducing species TPrA• plays an important role in the ECL mechanism of the $Ru(bpy)_3^{2+}$/TPrA system according to the literature [52]. It was consistent with the fact that the short-lived TPrA radical cation ($TPrA•^+$) is believed to lose a proton from the R-carbon to form the TPrA• in the partial alkaline condition [52]. Considering the survival condition of ssDNA and CdkN2A/p16 anti-oncogene, pH 7.2 was selected as the optimized pH value of PBS at the following experiment.

3.6. The calibration curve of CdkN2A/p16 anti-oncogene detection

The sensitivity of the ECL biosensor was investigated. ECL responses for various dsDNA electrodes are shown in Fig. 7. The ECL intensity difference [ΔI_{ECL}, $\Delta I_{ECL} = I_{ECL} - I^0_{ECL}$(blank)] of the dsDNA electrodes grew when the CdkN2A/p16 anti-oncogene concentration increased, and the ΔI_{ECL} was found to be linear with the logarithm of CdkN2A/p16 anti-oncogene concentration in the range from 1 fM to 1 pM (as shown in the inset). The equation for the resulting calibration plot was $y = 191.8x + 431.3$ (x was the log concentration of CdkN2A/p16 anti-oncogene in log fM, y was the ΔI_{ECL}), the correlation coefficient was 0.9993, and a detection limit of 0.5 fM was estimated by using 3σ (where σ is the relative standard deviation of a blank solution, n=11). The consistent data was obtained as shown in the error bar in the inset of the Fig. 7 when the experiment was repeated three times.

4. Conclusions

In summary, an ECL biosensor based on functional electrospun nanofibers for sensitive detection of CdkN2A/p16 anti-oncogene *via* binding luminescent composite nanoparticles for signal amplification has been designed. The PA6-MWCNTs-SiO_2 electrode with unique 3D nanostructure, large specific surface area and good biocompatibility (amino-functionalized) served as the supporting scaffold, which could not only firmly immobilize the ssDNA sequence *via* covalent linkage, but also significantly increase the amount of the ssDNA. RuAg@AuNPs exhibited excellent ECL behaviors on GCE with assistance of AgNPs, and are good DNA label. In fact, the combination of functional electrospun nanofibers and core-shell luminescent composite nanoparticles can result in enormous signal amplification, and thereby, it makes the ECL biosensor achieve high sensitivity. The biosensor displayed wide linear range, high sensitivity and good stability. The assay allows detection limit as low as 0.5 fM of CdkN2A/p16 anti-oncogene, which is comparable or better than that in reported anti-oncogene assays. The excellent analytical performances make the developed ECL biosensor a promising tool for the detection of many kinds of biomolecules at trace level, such as DNA, RNA and protein, etc.

Acknowledgments

Project supported by the National Nature Science Foundation of China (No. 81302472 and 81573313), the Fundamental Research Funds for the Central Universities (No. 2242017K41018) and the practice Innovation plans of postgraduates in Jiangsu Province (SJLX16_0076).

References

[1] A. Kamb, N.A. Gruis, J. Weaverfeldhaus, Q.Y. Liu, K. Harshman, S.V. Tavtigian, E. Stockert, R.S. Day, B.E. Johnson, M.H. Skolnick, A cell-cycle regulator potentially involved in genesis of many tumor types, Science 264 (1994) 436-440.

[2] C.F. Meng, X.J. Zhu, G. Peng, D.Q. Dai, Promoter histone H3 lysine 9 di-methylation is associated with DNA methylation and aberrant expression of p16 in gastric cancer cells, Oncol. Rep. 22 (2009) 1221-1227.

[3] M.J. Baker, A.M. Goldstein, P.L. Gordon, K.S. Harbaugh, H.B. Mackley, M.J. Glantz, J.J.

Drabick, An interstitial deletion within 9p21.3 and extending beyond CDKN2A predisposes to melanoma, neural system tumours and possible haematological malignancies, J. Med. Genet. 53 (2016) 721-727.

[4] M.R. Sargen, S.L. Merrill, E.Y. Chu, K.L. Nathanson, CDKN2A mutations with put loss predisposing to multiple nerve sheath tumours, melanoma, dysplastic naevi and internal malignancies: a case series and review of the literature, Brit. J. Dermatol. 175 (2016) 785-789.

[5] S.W. Aesif, M.C. Aubry, E.S. Yi, S.M. Kloft-Nelson, S.M. Jenkins, G.M. Spears, P.T. Greipp, W.R. Sukov, A.C. Roden, Loss of p16(INK4A) expression and homozygous CDKN2A deletion are associated with worse outcome and younger age in thymic carcinomas, J. Thorac. Oncol. 12 (2017) 860-871.

[6] Z. Zhu, T. Liu, F. Han, S.D. Zhan, C.Y. Wang, Mutations in the p16 gene in DMBA-induced pancreatic intraepithelial neoplasia and pancreatic cancer in rats, Hepatob. Pancreatic. Dis. Int. 14 (2015) 208-214.

[7] A.L. Vestergaard, K. Thorup, U.B. Knudsen, T. Munk, H. Rosbach, J.B. Poulsen, P. Guldberg, P.M. Martensen, Oncogenic events associated with endometrial and ovarian cancers are rare in endometriosis, Mol. Hum. Reprod. 17 (2011) 758-761.

[8] A. Mokrowiecka, A. Wierzchniewska-Lawska, B. Smolarz, H. Romanowicz-Makowska, E. Malecka-Panas, p16 gene mutations in Barrett's esophagus in gastric metaplasia - intestinal metaplasia - dysplasia - adenocarcinoma sequence, Adv. Med. Sci. 57 (2012) 71-76.

[9] M.K. Sibin, D.I. Bhat, C. Lavanya, M.J. Manoj, S. Aakershita, G.K. Chetan, CDKN2A exon-wise deletion status and novel somatic mutations in Indian glioma patients, Tumor Biol. 35 (2014) 1467-1472.

[10] I.M. Schaefer, J.L. Hornick, L.M. Sholl, B.J. Quade, M.R. Nucci, C. Parra-Herran, Abnormal p53 and p16 staining patterns distinguish uterine leiomyosarcoma from inflammatory myofibroblastic tumour, Histopathology 70 (2017) 1138-1146.

[11] C.W. Ge, W.J. Miao, M.J. Ji, N. Gu, Glutaraldehyde-modified electrode for nonlabeling voltammetric detection of p16(INK4A) gene, Anal. Bioanal. Chem. 383 (2005) 651-659.

[12] W.T. Xu, N. Cheng, K.L. Huang, Y.H. Lin, C.G. Wang, Y.C. Xu, L.J. Zhu, D. Du, Y.B. Luo, Accurate and easy-to-use assessment of contiguous DNA methylation sites based on

proportion competitive quantitative-PCR and lateral flow nucleic acid biosensor, Biosens. Bioelectron. 80 (2016) 654-660.

[13] L. Yang, X.H. Huang, L. Sun, L. Xu, A piezoelectric immunosensor for the rapid detection of p16(INK4a) expression in liquid-based cervical cytology specimens, Sensor. Actuat. B-Chem. 224 (2016) 863-867.

[14] K. Chen, M.Y. Zhang, Y.N. Chang, L. Xia, W.H. Gu, Y.X. Qin, J. Li, S.X. Cui, G.M. Xing, Utilizing gold nanoparticle probes to visually detect DNA methylation, Nanoscale Res. Lett. 11 (2016) 304-313.

[15] L. Xiao, L. Xu, C. Gao, Y.L. Zhang, Q.F. Yao, G.J. Zhang, A MoS_2 nanosheet-based fluorescence biosensor for simple and quantitative analysis of DNA methylation, Sensors 16 (2016), 1561-1570.

[16] P. Hou, M.J. Ji, C.W. Ge, J.Y. Shen, S. Li, N.Y. He, Z.H. Lu, Detection of methylation of human p16(Ink4a) gene 5 '-CpG islands by electrochemical method coupled with linker-PCR, Nucleic Acids Res. 31 (2003) 92-98.

[17] H.D. Zhang, L.F. Shan, X.N. Wang, Q. Ma, J. Fang, A novel bisulfite-microfluidic temperature gradient capillary electrophoresis platform for highly sensitive detection of gene promoter methylation, Biosens. Bioelectron. 42 (2013) 503-511.

[18] P. Duangkaew, S. Tapaneeyakorn, C. Apiwat, T. Dharakul, S. Laiwejpithaya, P. Kanatharana, R. Laocharoensuk, Ultrasensitive electrochemical immunosensor based on dual signal amplification process for p16(INK4a) cervical cancer detection in clinical samples, Biosens. Bioelectron. 74 (2015) 673-679.

[19] M.M. Richter, Electrochemiluminescence (ECL), Chem. Rev. 104 (2004) 3003-3036.

[20] Z.Y. Liu, W.J. Qi, G.B. Xu, Recent advances in electrochemiluminescence, Chem. Soc. Rev. 44 (2015) 3117-3142.

[21] X.J. Li, Y.G. Wang, L. Shi, H.M. Ma, Y. Zhang, B. Du, D. Wu, Q. Wei, A novel ECL biosensor for the detection of concanavalin A based on glucose functionalized $NiCo_2S_4$ nanoparticles-grown on carboxylic graphene as quenching probe, Biosens. Bioelectron. 96 (2017) 113-120.

[22] G.F. Jie, L. Tan, Y. Zhao, X.C. Wang, A novel silver nanocluster in situ synthesized as versatile probe for electrochemiluminescence and electrochemical detection of thrombin by

multiple signal amplification strategy, Biosens. Bioelectron. 94 (2017) 243-249.

[23] Q. Liu, C. Ma, X.P. Liu, Y.P. Wei, C.J. Mao, J.J. Zhu, A novel electrochemiluminescence biosensor for the detection of microRNAs based on a DNA functionalized nitrogen doped carbon quantum dots as signal enhancers, Biosensors. Bioelectron. 92 (2017) 273-279.

[24] A. Ravalli, D. Voccia, I. Palchetti, G. Marrazza, Electrochemical, electrochemiluminescence, and photoelectrochemical aptamer-based nanostructured sensors for biomarker analysis, Biosensors 6 (2016) 39-58.

[25] Y. Chen, S.W. Zhou, L.L. Li, J.J. Zhu, Nanomaterials-based sensitive electrochemiluminescence biosensing, Nano Today 12 (2017) 98-115.

[26] Z. Aytac, Z.I. Yildiz, F. Kayaci-Senirmak, T. Tekinay, T. Uyar, Electrospinning of cyclodextrin/linalool-inclusion complex nanofibers: Fast-dissolving nanofibrous web with prolonged release and antibacterial activity, Food Chem. 231 (2017) 192-201.

[27] A. Yamakawa, S. Suzuki, T. Oku, K. Enomoto, M. Ikeda, J. Rodrigue, K. Tateiwa, Y. Terada, H. Yano, S. Kitamura, Nanostructure and physical properties of cellulose nanofiber-carbon nanotube composite films, Carbohyd. polym. 171 (2017) 129-135.

[28] Q.H. Guo, L.J. Liu, M. Zhang, H.Q. Hou, Y.H. Song, H.D. Wang, B.Y. Zhong, L. Wang, Hierarchically mesostructured porous TiO_2 hollow nanofibers for high performance glucose biosensing, Biosens. Bioelectron. 92 (2017) 654-660.

[29] E. Sapountzi, M. Braiek, F. Vocanson, J.F. Chateaux, N. Jaffrezic-Renault, F. Lagarde, Gold nanoparticles assembly on electrospun poly(vinyl alcohol)/poly(ethyleneimine)/glucose oxidase nanofibers for ultrasensitive electrochemical glucose biosensing, Sens. Actuator B-Chem. 238 (2017) 392-401.

[30] K. Mondal, M.A. Ali, C. Singh, G. Sumana, B.D. Malhotra, A. Sharma, Highly sensitive porous carbon and metal/carbon conducting nanofiber based enzymatic biosensors for triglyceride detection, Sensor. Actuat. B-Chem. 246 (2017) 202-214.

[31] S. Tripathy, S.R.K. Vanjari, V. Singh, S. Swaminathan, S.G. Singh, Electrospun manganese (III) oxide nanofiber based electrochemical DNA-nanobiosensor for zeptomolar detection of dengue consensus primer, Biosens. Bioelectron. 90 (2017) 378-387.

[32] G. Kabay, G.K. Can, M. Mutlu, Amyloid-like protein nanofibrous membranes as a sensing layer infrastructure for the design of mass-sensitive biosensors, Biosens. Bioelectron. 97

(2017) 285-291.

[33] X.Y. Wang, Y.J. Wang, M. Jiang, Y.Q. Shan, X.B. Wang, On-site determination of bisphenol A in river water by a novel solid-state electrochemiluminescence quenching sensor, Environ. Chem. 14 (2017) 115-122.

[34] X.Y. Wang, X.B. Wang, S.M. Gao, Y. Zheng, M. Tang, B.A. Chen, A solid-state electrochemiluminescence sensing platform for detection of catechol based on novel luminescent composite nanofibers, Talanta 107 (2013) 127-132.

[35] X.Y. Wang, X. Wang, X. Wang, F. Chen, K. Zhu, Q. Xu, M. Tang, Novel electrochemical biosensor based on functional composite nanofibers for sensitive detection of p53 tumor suppressor gene, Anal. Chim. Acta 765 (2013) 63-69.

[36] X. Wang, G. Shu, C. Gao, Y. Yang, Q. Xu, M. Tang, Electrochemical biosensor based on functional composite nanofibers for detection of K-ras gene *via* multiple signal amplification strategy, Anal. Biochem. 466 (2014) 51-58.

[37] X.Y. Wang, C.C. Gao, G.F. Shu, Y.J. Wang, X.G. Liu, The enzyme electrocatalytic immunosensor based on functional composite nanofibers for sensitive detection of tumor suppressor protein p53, J. Electroanal. Chem. 756 (2015) 101-107.

[38] X.M. Yang, X. Li, L.Z. Zhang, J.M. Gong, Electrospun template directed molecularly imprinted nanofibers incorporated with BiOI nanoflake arrays as photoactive electrode for photoelectrochemical detection of triphenyl phosphate, Biosens. Bioelectron. 92 (2017) 61-67.

[39] D.P. Tang, R. Yuan, Y.Q. Chai, Ligand-functionalized core/shell Ag@Au nanoparticles label-Free amperometric immun-biosensor, Biotechnol. Bioeng. 94 (2006) 996-1004.

[40] H. Cai, Y. Xu, N.N. Zhu, P.G. He, Y.Z. Fang, an electrochemical DNA hybridization detection assay based on a silver nanoparticle label, Analyst 127 (2002) 803-808.

[41] M. Qhobosheane, S. Santra, P. Zhang, W.H. Tan, Biochemically functionalized silica nanoparticles, Analyst 126 (2001) 1274-1278.

[42] X.Y. Wang, J.M. Zhou, W. Yun, S.S. Xiao, Z. Chang, P.G. He, Y.Z. Fang, Detection of thrombin using electrogenerated chemiluminescence based on $Ru(bpy)_3^{2+}$-doped silica nanoparticle aptasensor *via* target protein-induced strand displacement, Anal. Chim. Acta 598 (2007) 242-248.

[43] Y. Zhang, F.F. Wen, J. Tan, C. Jiang, M. Zhu, Y.J. Chen, H.G. Wang, Highly efficient electrocatalytic oxidation of nitrite by electrodeposition of Au nanoparticles on molybdenum sulfide and multi-walled carbon nanotubes, J. Electroanal. Chem. 786 (2017) 43-49.

[44] B.M. Huang, X.B. Zhou, Z.H. Xue, X.Q. Lu, Electrochemiluminescence quenching of tris(2,2´-bipyridyl)ruthenium, Trends Anal. Chem. 51 (2013) 107-116.

[45] W.J. Miao, J.P. Choi, A.J. Bard, Electrogenerated chemiluminescence 69: the tris(2,2′-bipyridine)ruthenium(II), ($Ru(bpy)_3^{2+}$)/tri-*n*-propylamine (TPrA) system revisited-a new route involving $TPrA^{\bullet+}$ cation radicals, J. Am. Chem. Soc. 124 (2002) 14478-14485.

[46] X.Q. Lu, L. Wang, D. Liu, J. Du, H.F. Wang, Cathodic electrochemiluminescence of tris(2,2′-bipyridine) ruthenium(II) on Ag nanoparticles-modified electrode, J. Electroanal. Chem. 702 (2013) 60-65.

[47] X.Y. Wang, Y.J. Wang, M. Jiang, Y.Q. Shan, X. Jin, M. Gong, X.N. Wang, Functional electrospun nanofibers-based electrochemiluminescence immunosensor for detection of the TSP53 using RuAg/SiO_2NPs as signal enhancers, Anal. Biochem. 548 (2018) 15-22.

[48] G. Herzog, E. Sibottier, M. Etienne, A. Walcarius, Electrochemically assisted self-assembly of ordered and functionalized mesoporous silica films: impact of the electrode geometry and size on film formation and properties, Faraday Discuss. 164 (2013) 259-273.

[49] S. Sayen, A. Walcarius, Electro-assisted generation of functionalized silica films on gold, Electrochem. Commun. 5 (2003) 341-348.

[50] X.Y. Wang, X.Y. Zhang, P.G. He, Y.Z. Fang, Sensitive detection of p53 tumor suppressor gene using an enzyme-based solid-state electrochemiluminescence sensing platform, Biosens. Bioelectron. 26 (2011) 3608-3613.

[51] Y. Dror, W. Salalha, R.L. Khalfin, Y. Cohen, A.L. Yarin, E. Zussman, Carbon nanotubes embedded in oriented polymer nanofibers by electrospinning, Langmuir 19 (2003) 7012-7020.

[52] W.J. Miao, J.P. Choi, A.J. Bard, Electrogenerated chemiluminescence 69: The tris(2,2 '-bipyridine)ruthenium(II), ($Ru(bpy)_3^{2+}$)/tri-n-propylamine (TPrA) system revisited - A new route involving TPrA(center dot+) cation radicals, J. Am. Chem. Soc. 124 (2002), 14478-14485.

Table 1. Oligonucleotide sequences used in the experiment.

Table 2. The electrochemical surface areas of various electrodes.

Fig. 1. Schematic representation of the preparation of the ECL biosensor.

Fig. 2. (A) TEM image of RuAg@AuNPs, Inset: the fluorescence photograph of RuAg@AuNPs. (B) The DPV curves for the RuAg@AuNPs (100 μL, curve a) and the $Ru(bpy)_3^{2+}$ solution (40 μM, curve b) in 10 mM PBS (pH 7.2). Scan range: 0.6~1.2 V (vs. Ag/AgCl), pulse amplitude: 0.05 V, pulse width: 0.05 s and pulse period: 0.2 s. Inset: The ECL intensity-time curves of the RuAg@AuNPs in 10 mM PBS containing 1.0 mM TPrA (pH 7.2). (C) The ECL intensity-potential curves of RuAg@AuNPs (a) and Ru@AuNPs (b) in 10 mM PBS containing 1.0 mM TPrA (pH 7.2).

Fig. 3. (A) FESEM image of the PA6-MWCNTs-SiO_2 electrode, Inset: FESEM image of the PA6-MWCNTs electrospun nanofibers. (B) The diameter distribution of the PA6-MWCNTs-SiO_2 functional electrospun nanofibers, Inset: the diameter distribution of the PA6-MWCNTs electrospun nanofibers. (C) The ECL intensity-time curves of the electrodes in 10 mM PBS containing 1.0 mM TPrA (pH 7.2), RuAg@Au-dsDNA/ SiO_2 electrode (a), Ru@Au-dsDNA/PA6-MWCNTs-SiO_2 electrode (b) and RuAg@Au-dsDNA/ PA6-MWCNTs-SiO_2 electrode (c).

Fig. 4. (A) CV curves in 1 mM $[Fe(CN)_6]^{3-/4-}$ solution of the bare GCE (a), PA6-MWCNTs-SiO_2 electrode (b), PA6-MWCNTs electrode (c), ssDNA electrode (d) and dsDNA electrode (e). Scan rate: 0.05 V/s, scan range: -0.2 to 0.6 V. (B) Nyquist plots for the impedance measurement in 10 mM $[Fe(CN)_6]^{3-/4-}$ solution for the bare GCE (a), PA6-MWCNTs electrode (b), PA6-MWCNTs-SiO_2 electrode (c), ssDNA electrode (d), dsDNA electrode (e).

Fig. 5. (A) Repetitive CV curves of the ssDNA electrode in 1 mM $[Fe(CN)_6]^{3-/4-}$ solution with 20 continuous cyclic scans. Scan rate: 0.05 V/s, scan range: -0.2 to 0.6 V. Inset: the partial enlargement graph. (B) ECL responses for various dsDNA electrodes. The ssDNA electrodes were freshly prepared (a), after 7 days of storage at 4 ℃ (b), and the concentrations of CdkN2A/p16 anti-oncogene were 100 pM.

Fig. 6. ECL responses for various dsDNA electrodes: blank (a), 1 nM CdkN2A/p16 anti-oncogene (b), 1 nM one-base mismatched sequence (C/A mismatched) (c), 1 nM three-base mismatched

sequence (G/T, C/A, G/A mismatched) (d), and 1 nM non-complementation sequence (e).

Fig. 7. ECL responses for various dsDNA electrodes. The concentrations of CdkN2A/p16 anti-oncogene were 0 M (a), 1 fM (b), 10 fM (c), 100 fM (d), 1 pM (e), 10 pM (f), 100 pM (g), 1 nM (h) and 10 nM (i). Inset: Related calibration plot versus CdkN2A/p16 anti-oncogene concentrations in a range from 1 fM to 1 pM.

Scheme 1. Schematic illustration of the ECL mechanisms of the RuAg@AuNPs system.

Note: We hope that all **Figures** will appear in color on the Web and submit to the reviewers, but in black and white in the printed version.

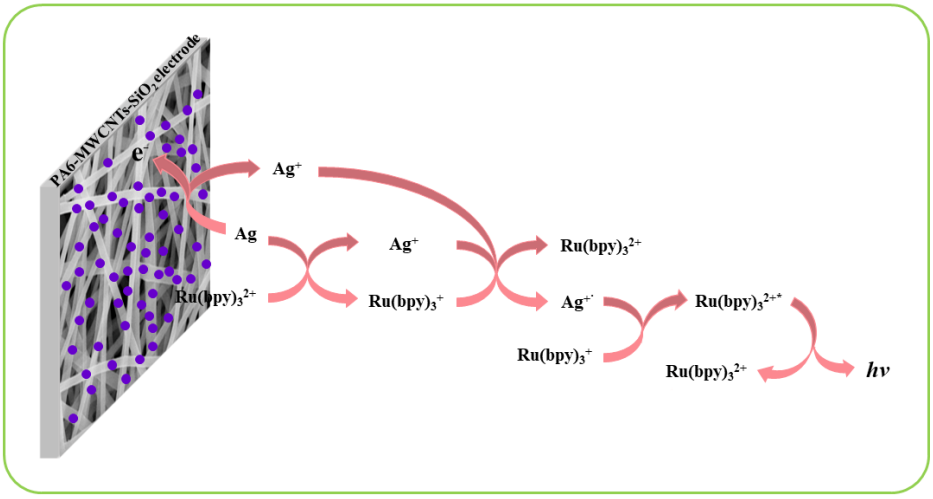

Scheme 1.

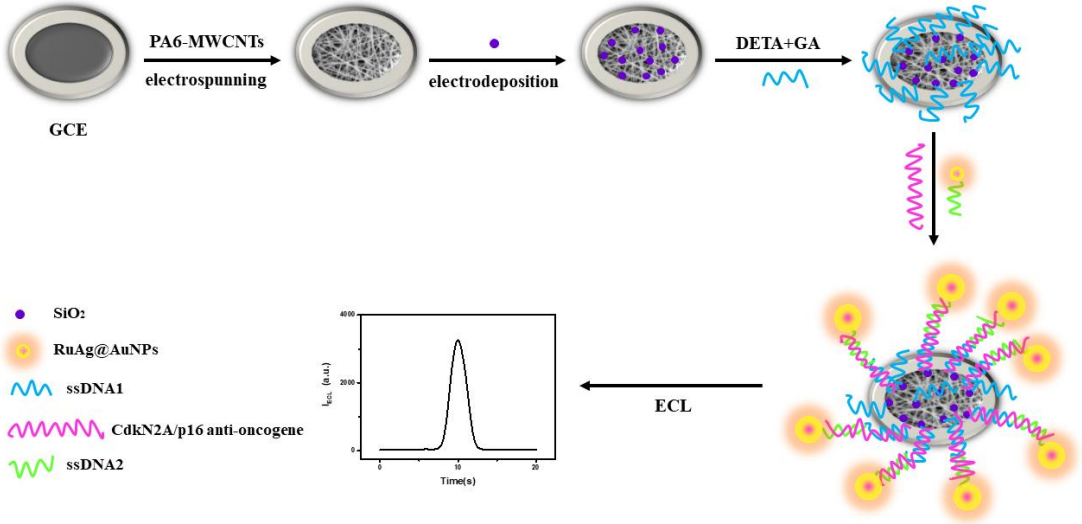

Fig. 1.

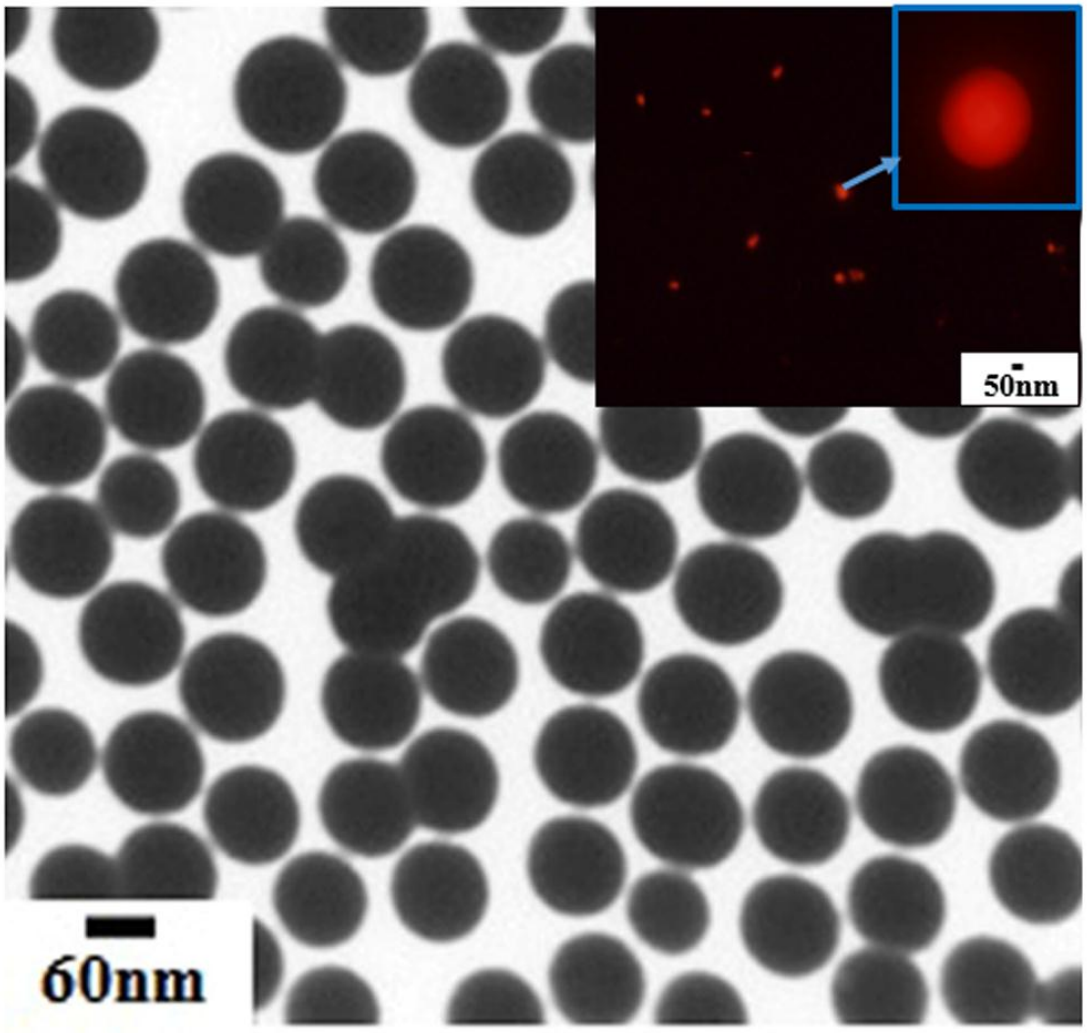

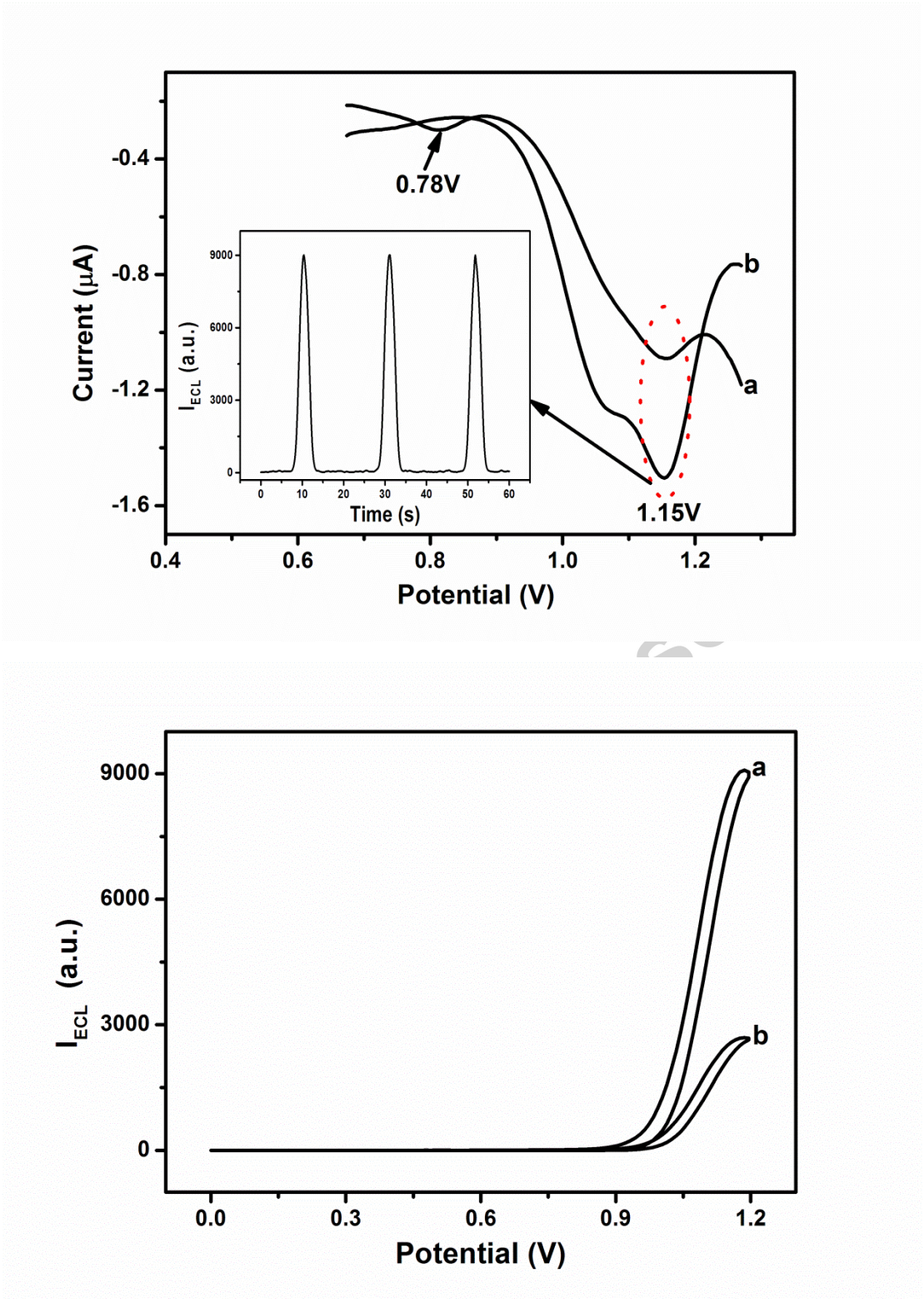
Current (μA)
-0.4
-0.8
-1.2
-1.6
0.4
0.6
0.8
1.0
1.2
Potential (V)
0.78V
1.15V
a
b
I_{ECL} (a.u.)
9000
6000
3000
0
0
10
20
30
40
50
60
Time (s)
I_{ECL} (a.u.)
9000
6000
3000
0
0.0
0.3
0.6
0.9
1.2
Potential (V)
a
b

Fig. 2.

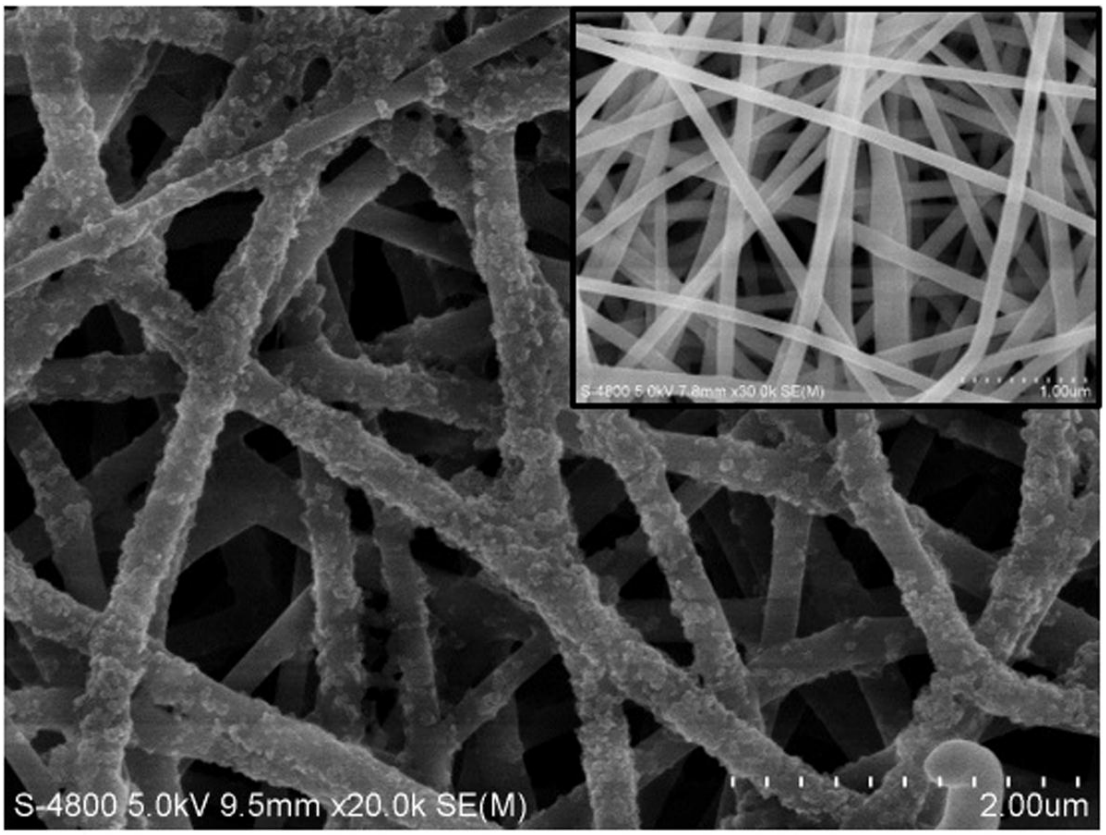
S-4800 5.0kV 9.5mm x20.0k SE(M)
2.00um

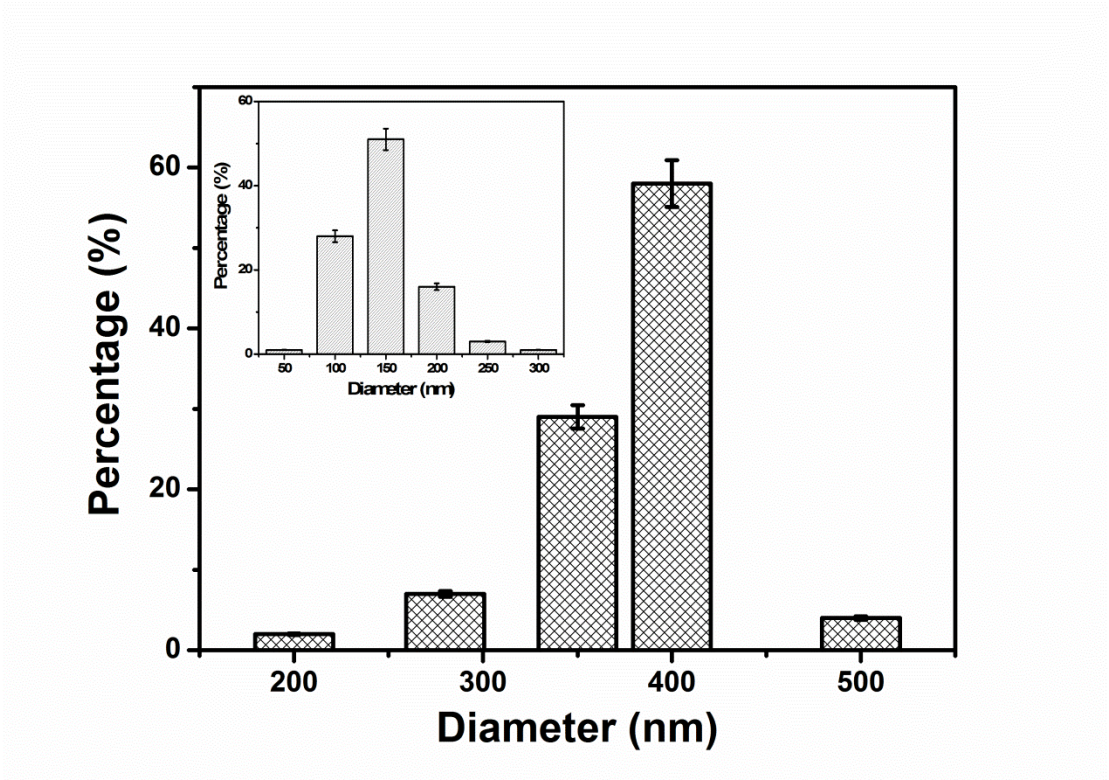
Percentage (%)
Diameter (nm)
0
20
40
60
200
300
400
500
Percentage (%)
Diameter (nm)
50
100
150
200
250
300

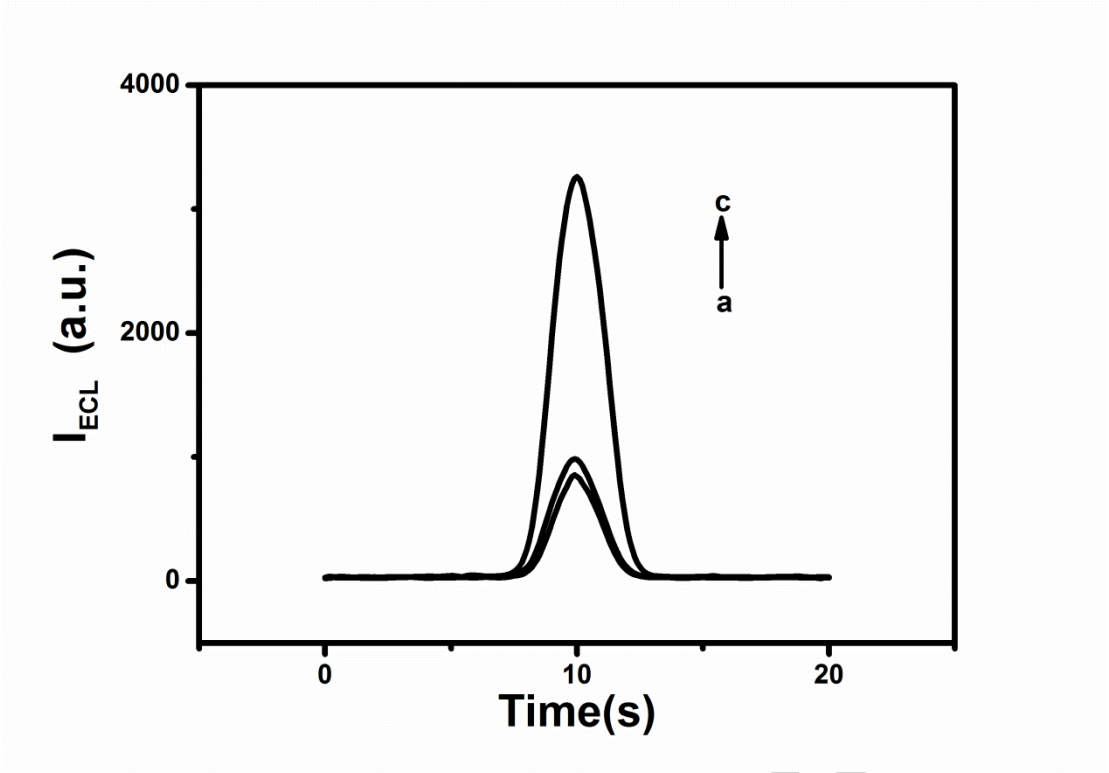

Fig. 3.

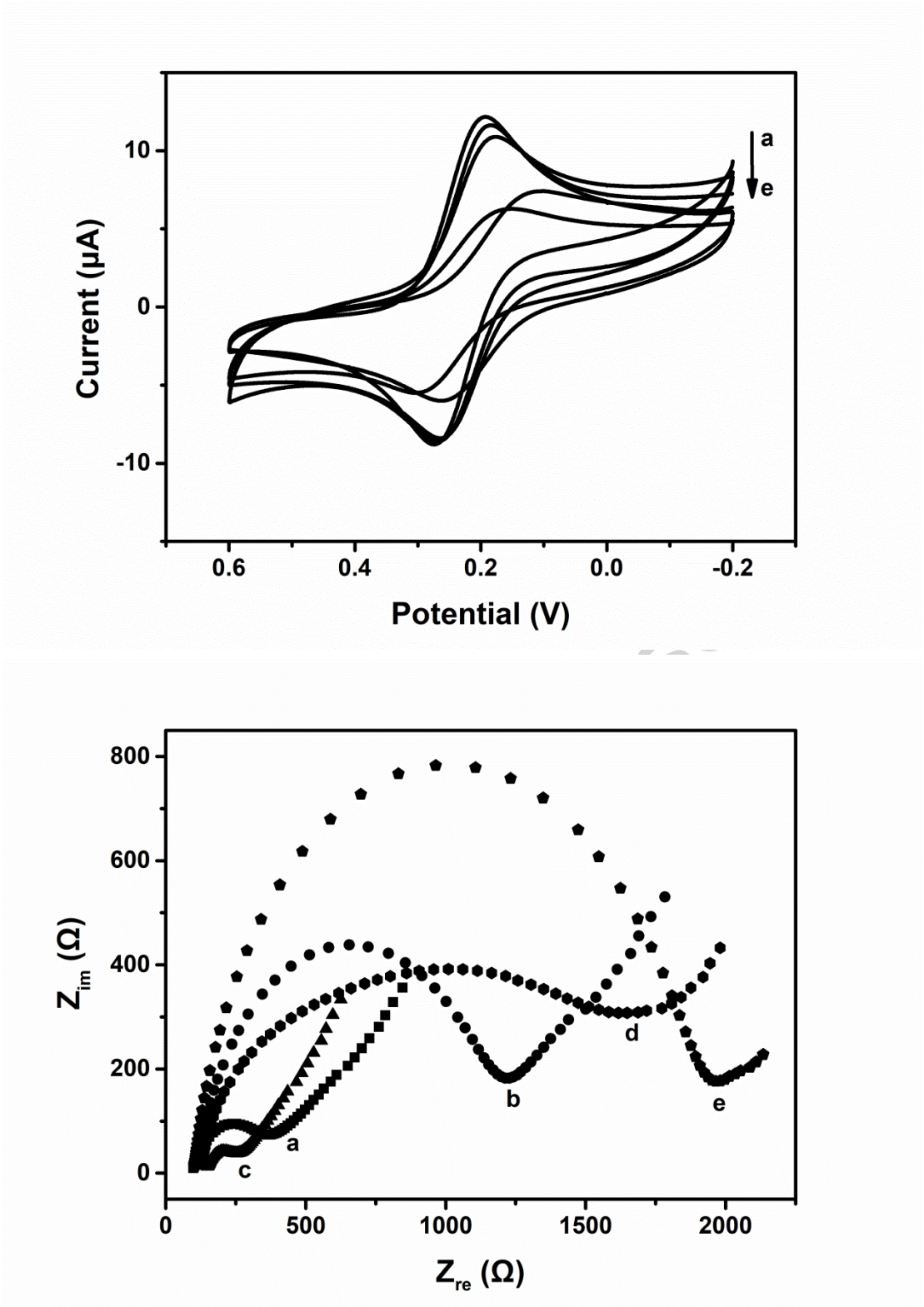
10
0
-10
Current (μA)
0.6
0.4
0.2
0.0
-0.2
Potential (V)
a
e
800
600
400
200
0
Z_{im} (Ω)
0
500
1000
1500
2000
Z_{re} (Ω)
a
b
c
d
e

Fig. 4.

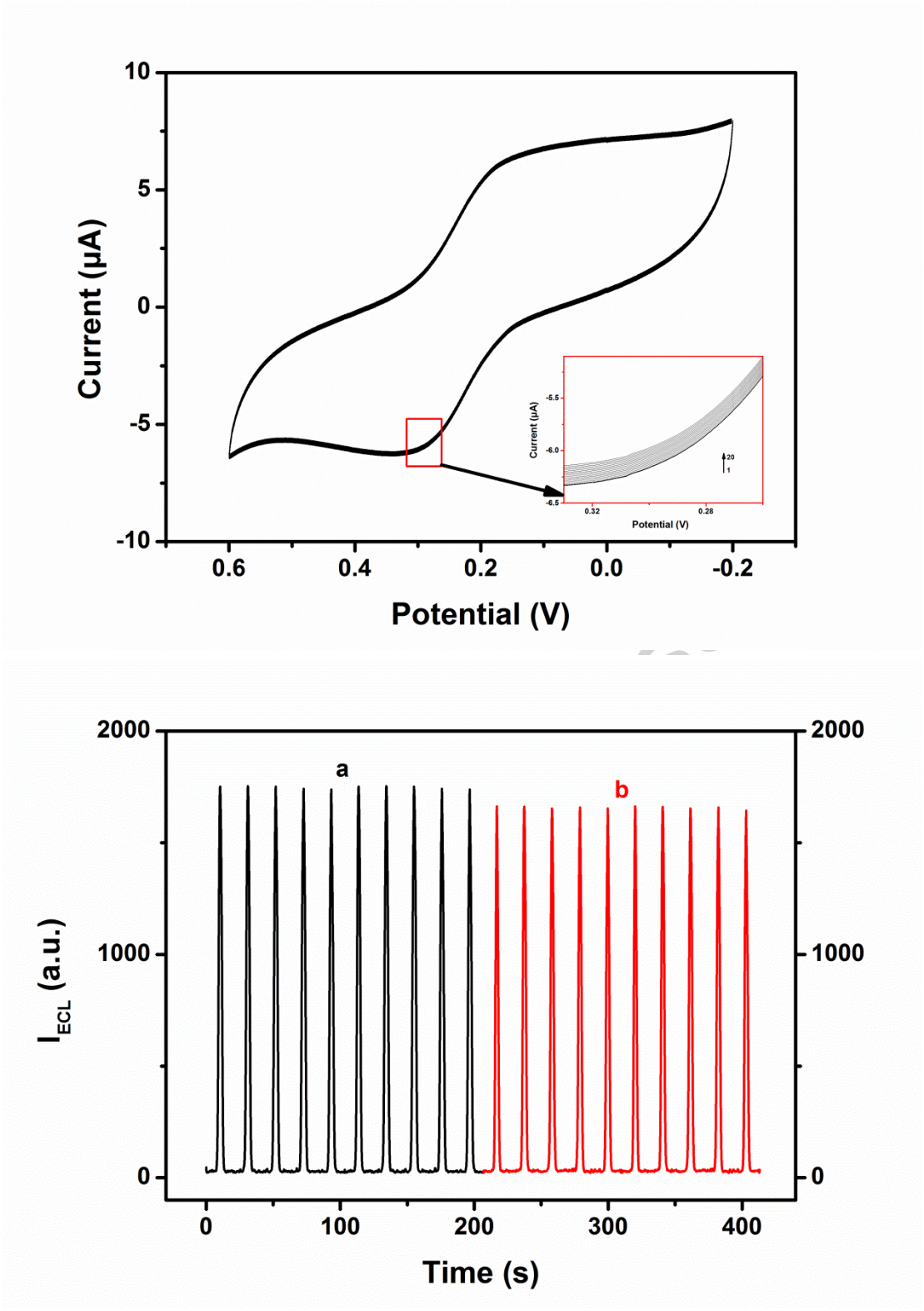
Current (μA)
Potential (V)
10
5
0
-5
-10
0.6
0.4
0.2
0.0
-0.2
Current (μA)
-5.5
-6.0
-6.5
0.32
0.28
Potential (V)
20
1
I_{ECL} (a.u.)
2000
1000
0
a
b
0
100
200
300
400
Time (s)

Fig. 5.

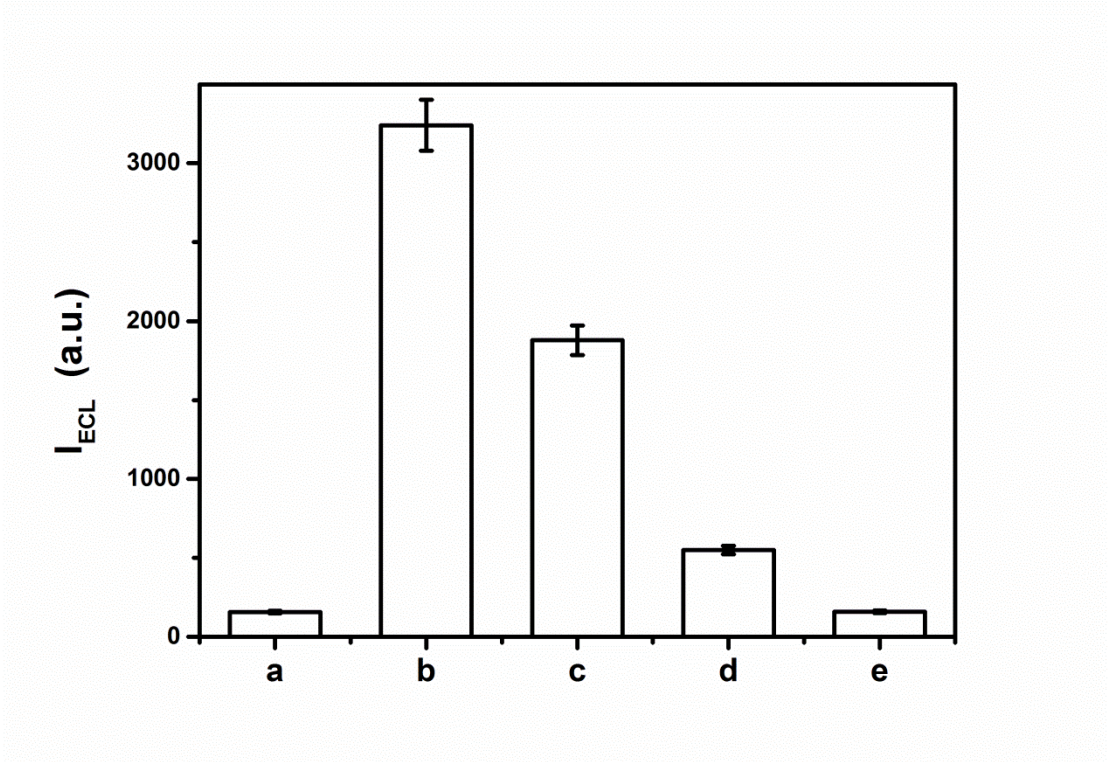
3000
2000
1000
0
I_{ECL} (a.u.)
a
b
c
d
e

Fig. 6.

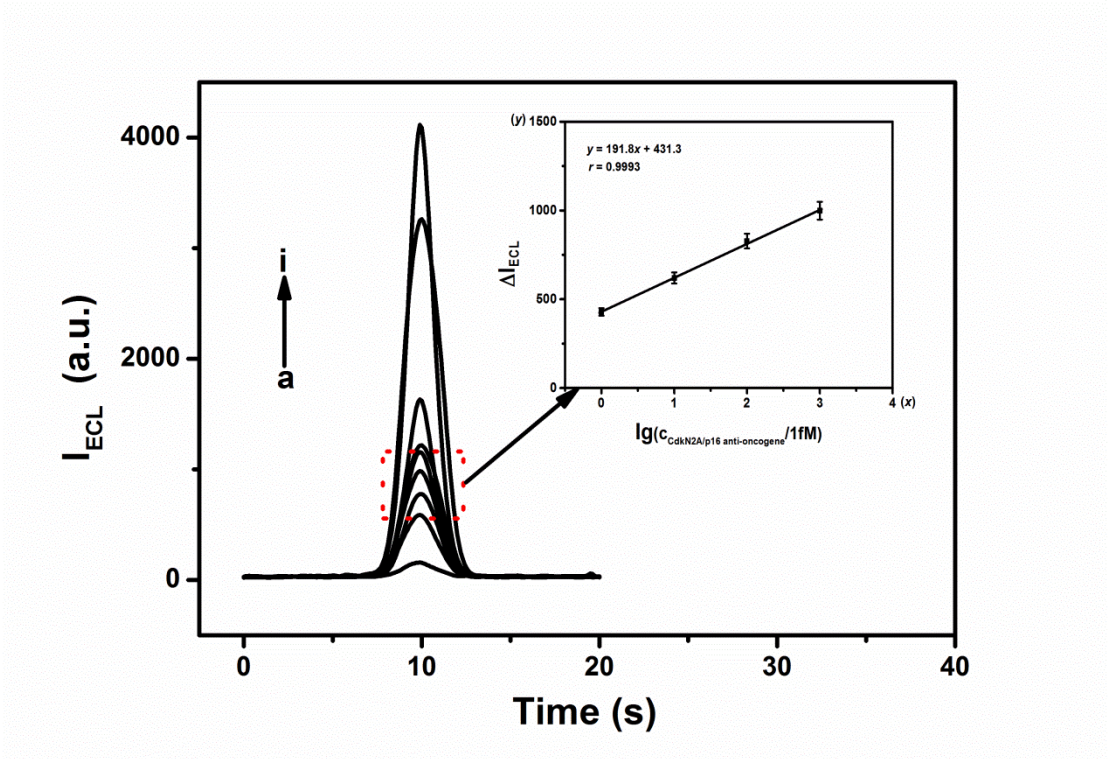
4000
2000
0
I_{ECL} (a.u.)
i
a
0
10
20
30
40
Time (s)
(y) 1500
1000
500
0
ΔI_{ECL}
y = 191.8x + 431.3
r = 0.9993
0
1
2
3
4 (x)
lg($c_{CdkN2A/p16\ anti\text{-}oncogene}$/1fM)

Fig. 7.

Table 1. Oligonucleotide sequences used in the experiment.

Primer	Sequence 5'-3'
CdkN2A/p16 anti-oncogene	ATTTAGGTAGCGGGCGGCTAG
ssDNA1	H_2N-CTAGCCGCCCGC
ssDNA2	TACCTAAAT-SH
[a] one-base mismatch	ATTTAGGTAG*A*GGGCGGCTAG
[a] three-base mismatch	ATTTA*T*GTAG*A*GGGCG*A*CTAG
non-complementation	CCCTTCACGTATTTAAAGCCA

[a] The underlined red bases are mismatched ones.

Table 2 The electrochemical surface areas of various electrodes.

Parameter	**bare GCE**	**SiO_2/GCE**	**PA6-MWCNTs-SiO_2/GCE**
A(cm^2)	**0.071**	**0.171**	**0.684**

Highlights:

- The functional electrospun nanofibers (PA6-MWCNTs-SiO_2) were first fabricated by electrospinning/electrodeposition technique.
- It is the first ECL biosensor based on PA6-MWCNTs-SiO_2 to detect the CdkN2A/p16 anti-oncogene at trace level.
- The core-shell luminescent composite nanoparticles (RuAg@AuNPs) as DNA label can dramatically amplify the ECL signal and enhance the sensitivity of detection.
- The detection limit for p16 is 0.5 fM, which is comparable or better than that in reported anti-oncogene assays.